Journal of Ceramic Processing Research. Vol. 21, No. 2, pp. 249~255 (2020)
(Received 25 December 2019, Received in revised form 30 March 2020, Accepted 2 April 2020)
https://doi.org/10.36410/jcpr.2020.21.2.249

J O U R N A L O F
Ceramic Processing Research

Influence of codeposited Al_2O_3 and h/BN on tribological properties of Ni-Al_2O_3-h/BN composite coatings

Jin-Hyuk Choi[a], Gobinda Gyawali[b,*], Dhani Ram Dhakal[c], Sami Bin Humam[c], Bhupendra Joshi[b] and Soo Wohn Lee[c,*]

[a]*Research Center for Eco Multifunctional Nano Materials, Sun Moon University, Asan, Korea*
[b]*Department of Fusion Science and Technology, Sun Moon University, Asan, Korea*
[c]*Department of Environmental and Bio-Chemical Engineering, Sun Moon University, Asan, Korea*

Ni-Al_2O_3-h/BN composite coatings were prepared by dispersing different contents of Al_2O_3 nanoparticles and h/BN nanosheets in the plating bath. The prepared composite coatings were then characterized for surface morphology, surface roughness, elemental composition, Vickers microhardness, X-ray diffraction, and wear and coefficient of friction test by using modern instruments. Compared to the nickel coating, composite coatings have revealed an increase in Vickers microhardness, improved surface roughness, and tribological properties. Increasing the h/BN content into the deposit improved the coefficient of friction, whereas increase in Al_2O_3 content improved wear rate. Among the different samples, the composite coating prepared by dispersing 10 g/L of each Al_2O_3 nanoparticles and h/BN nanosheets improved both wear and coefficient of friction under dry condition. In addition, the coefficient of friction was also investigated under different loadings during the wear test. The result showed that the lowest coefficient of friction was observed at 5 N load.

Keywords: Ni-Al_2O_3-h/BN composite coating, Hardness, Wear, Coefficient of friction.

Introduction

Electrodeposition offers a low-cost fabrication of metallic coatings over weak substrates for improving mechanical properties, and protection against wear and electrochemical corrosion [1]. Nickel is one of the most popular metallic coatings for engineering purposes. Nickel electroplating technology has been extensively progressed during the last 50 years to produce a wide range of industrial coatings for decorative, protective as well as functional properties [2]. In addition to its remarkable brightness and lustrous appearance, it provides a unique combination of corrosion and wear resistance.

Metal matrix composite coatings have gained much interest in recent years due to their improved coating properties as compared to single metal or alloy plating [3]. Electrodeposition of metal matrix composites is applied to produce wear and corrosion resistant coatings; however, the properties of these coatings mainly depend on their composition and structure [4, 5]. Different types of ceramic nanoparticles and 2D nanomaterials have been successfully incorporated into the metal matrix during electro/electroless deposition techniques for improved wear and corrosion resistance. Among different types of ceramics, carbides (SiC, TiC, B_4C, etc.), oxides (Al_2O_3, TiO_2, ZrO_2, CeO_2, etc.), and nitrides (Si_3N_4, TiN, AlN, etc.) ceramics [5-10] are extensively investigated as second phase reinforcements in the electrodeposited metal matrix composite system to elucidate electrical, catalytical, thermal, mechanical, tribological, and electrochemical corrosion properties. Similarly, 2D materials such as reduced graphene oxide [11], graphite [12], h-BN [13], MoS_2 [14], WS_2 [15], etc. are mainly studied for the tribological properties, especially to reduce coefficient of friction, and wear rate during the sliding contacts. Studies have revealed that the uniform distribution of ceramic particles into the metal matrix significantly improves the tribological and electrochemical properties of the coatings [15, 16]. Codeposition of Al_2O_3 nanoparticles into Ni coating has shown improvement in microhardness and corrosion resistant behavior of the coating [17]. Improvement in hardness is related to the dispersion hardening effect and load bearing capacity of the codeposited Al_2O_3 particles [18]. In addition, microstructural modification in the composite coating leading to grain refinement is another aspect for achieving a hard deposit.

On the other hand, h/BN nanosheets are regarded as the solid lubricating material due to their layered sheet structure. Hence, an improvement in coefficient of friction by reinforcement of h/BN has been reported [19]. The h/BN nanosheets are relatively soft by virtue of their layered crystal structure. Therefore, a significant improvement in microhardness of the composite coating was not achieved by the codeposition of a higher

*Corresponding author:
Tel : +82-41-530-2882
Fax: +82-41-530-2840
E-mail: ggobinda@sunmoon.ac.kr (G. Gyawali),
swlee@sunmoon.ac.kr (S. W. Lee)

amount of h/BN into the Ni electrodeposits [19, 20]. Therefore, a proper combination of hard type nanoparticles (e.g., Al_2O_3) and solid-lubricating 2D materials (e.g., h/BN nanosheets) could be the potential material to increase in both microhardness and tribological properties of the composite coating.

Therefore, the aim of the present study is to fabricate Ni-Al_2O_3-h/BN composite coatings containing different contents of Al_2O_3 and h/BN reinforcements via composite electrodeposition technique and investigate the combined effects of Al_2O_3 and h/BN particles on microstructural, mechanical, and tribological properties of the composite coatings.

Experimental

Preparation of Ni-Al_2O_3-h/BN composite coatings

The composite electrodeposition was carried out by using a pulse DC current technique. The composition and concentration of the electrolytic bath are shown in Table 1. Pure Ni balls in titanium basket was used as anode and a polished copper sheet of exposed area of 2.25 cm^2 as cathode. Different concentrations of Al_2O_3 nanoparticles and h/BN nanosheets were dispersed ultrasonically in the plating bath prior to the electrodeposition. A pulse DC current with 80 mA/cm^2 current density, 50% pulse duty cycles, and 100 Hz pulse frequency were adjusted during the electrodeposition. After electrodeposition, samples were cleaned in ultrasound to remove loosely adhered ceramic particles from the surface. The samples prepared by dispersing 5 g/L Al_2O_3 + 15 g/L h/BN, 10 g/L Al_2O_3 + 10 g/L h/BN, and 15 g/L Al_2O_3 + 5 g/L h/BN were referred as NiAl5BN15, NiAl10BN10, and NiAl15BN5, respectively. In all the composite coatings, the total amount of ceramic loading was fixed to 20 g/L. For a reference, pure nickel coating without ceramics loading was also prepared under similar conditions.

Characterizations

The samples thus prepared were characterized for microstructures and phase composition, surface morphology, surface roughness, and microhardness by using X-ray diffraction (XRD, Rigaku RINT 2200, X-Ray diffractometer, Japan), scanning electron microscope (SEM, Nanoeye, Korea), Surface roughness tester (Surftest), and Vickers microhardness tester (Buehler Ltd., USA), respectively. Vickers microhardness test was carried out for 10 replicates on the coating surface under 0.98 N load, and the values were averaged.

Tribological properties of the electrodeposited coatings were evaluated by reciprocal sliding test using ball on disc method Tribometer (CSM instruments; TRN 01-04879). A zirconia ball was used as the counterpart, while the electrodeposited coating was used as a disc. A constant load of 5 N was used with a sliding speed of 1.48 cm/s for 15 min under dry condition (at 23 °C and 30% humidity). Tribology test under different loading conditions (3 N, 5 N, 7.5 N and 10 N) was also carried out to investigate the variation of coefficient of friction at different loads. Coefficient of friction was recorded simultaneously during the wear test. The worn surfaces after the tribology test were observed by SEM to study the wear mechanism during the wear test.

Table 1. Electrodeposition parameters and operating conditions.

Compositions	Parameters
$Ni(NH_2SO_3)_2$ (g/L)	300
$NiCl_2$ (g/L)	10
H_3BO_3 (g/L)	40
Al_2O_3 (g/L)	5-15
h/BN (g/L)	5-15
CTAB (g/L)	0.2
SDS (g/L)	0.3
Temperature (°C)	50
pH	4.2
Current density (mA/cm^2)	80
Stirring rate (rpm)	200
Plating time (min)	60

Results and Discussion

Surface morphologies, XRD, and microstructures

Surface morphologies of the pure Ni, NiAl5BN15, NiAl10BN10, and NiAl15BN5 composite coatings are shown in Fig. 1. Variation in surface morphologies are observed depending on the amount and type of ceramic nanoparticles codeposition. Pure nickel (Fig. 1(a)) shows more or less homogeneous surface topography with pyramidal granules. On the other hand, composite coating NiAl10BN10 revealed finer surface topography as compared to NiAl5BN15 and NiAl15BN5 samples. In NiAl5BN15 sample, h/BN sheets are also clearly observed on the surface. However, in NiAl15BN5 sample, the morphology appears to be relatively rougher unlike other coatings. Reinforcement of second phase ceramic particles into the metal matrix during electrodeposition modifies the regular growth of the matrix grains. In other words, reduction of Ni ions into nickel is more or less obstructed by the codeposited ceramic particles during their regular growth, leading into smaller grains, and hence, changes the surface morphology. The average thickness of the coatings was measured to be 75 μm.

X-ray diffraction patterns of the Ni and Ni-Al_2O_3-h/BN composite coatings are shown in Fig. 2. A significant variation in relative peak intensities is found in the coatings. Compared to pure nickel coating, composite coatings possessed attenuation of (200) main reflection peak. In the FCC crystal structure of nickel coating, intense (200) reflection peak is also associated with the ductile behavior of the Ni coating [21]. Attenuation of (200) reflection peak and elevation of (311) peak

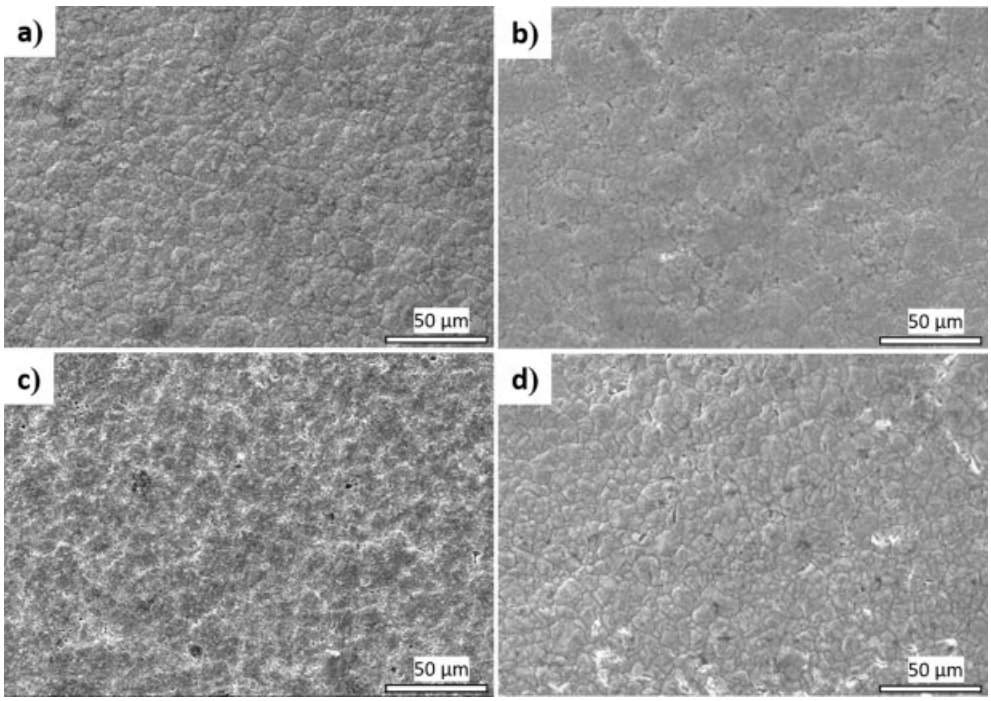

Fig. 1. SEM surface morphologies of (a) pure Ni, (b) NiAl15BN5, (c) NiAl10BN10, and (d) NiAl5BN15 samples.

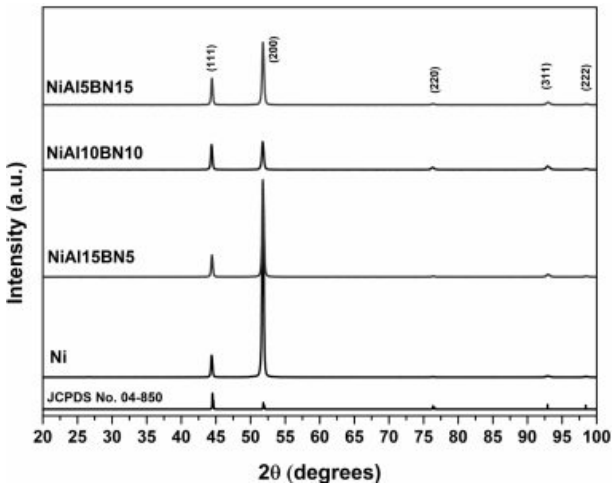

Fig. 2. X-ray diffraction patterns of the samples.

are associated with the mixed orientations of the nickel crystallites, suggesting a harder deposit. In the NiAl10BN10 sample, almost similar intensities of (111) and (200) peaks are observed. However, in all the composite coatings, the XRD peaks associated with the codeposited Al_2O_3 and h/BN are not detected. This might be due to the lower quantity of the reinforcements present in the coating, which is beyond the detection limit by XRD.

In order to investigate the distribution of codeposited ceramic particles into the nickel matrix, SEM cross-section observation was carried out, as shown in Fig. 3. Cross-section of NiAl15BN5 sample revealed mainly codeposited Al_2O_3 nanoparticles with less h/BN nanosheets, while NiAl5BN15 sample shows mainly co-deposited h/BN with low quantity of Al_2O_3 nanoparticles. Wt.% codeposition of Al_2O_3 and h/BN in the Ni coating is shown in Fig. 4. The result reveals that the codeposition of h/BN is more as compared to the Al_2O_3 nanoparticles. As the content of h/BN was increased in the plating bath, the codeposition wt.% of h/BN in the coating also increased. However, agglomerated h/BN nanosheet bundles are observed in the NiAl5BN15 sample (Fig. 3(d)). Studies have revealed that the agglomeration of second phase particles in the nickel matrix adversely affects the properties of the coating [22]. On the other hand, the sample NiAl10BN10 revealed a well distribution of both codeposited Al_2O_3 nanoparticles and h/BN nanosheets. The cross-section image of the reference nickel only coating possesses a fine appearance without any reinforcement phases, pores, or voids.

Microhardness

Vickers microhardness values of Ni and Ni-Al_2O_3-h/BN composite coatings are shown in Fig. 5. The average microhardness value of pure nickel coating is ~240 HV whereas, the Vickers microhardness of the Ni-Al_2O_3-h/BN composite coatings are above 450 HV. Vickers microhardness values of the composite coatings were increased by increasing the Al_2O_3 content and decreasing the h/BN content in the plating bath. The increase in microhardness is proportional to the increased codeposition wt.% of Al_2O_3 nanoparticles. However, Vickers microhardness of the composite coating vs. the content of h/BN in the plating bath revealed that the hardness

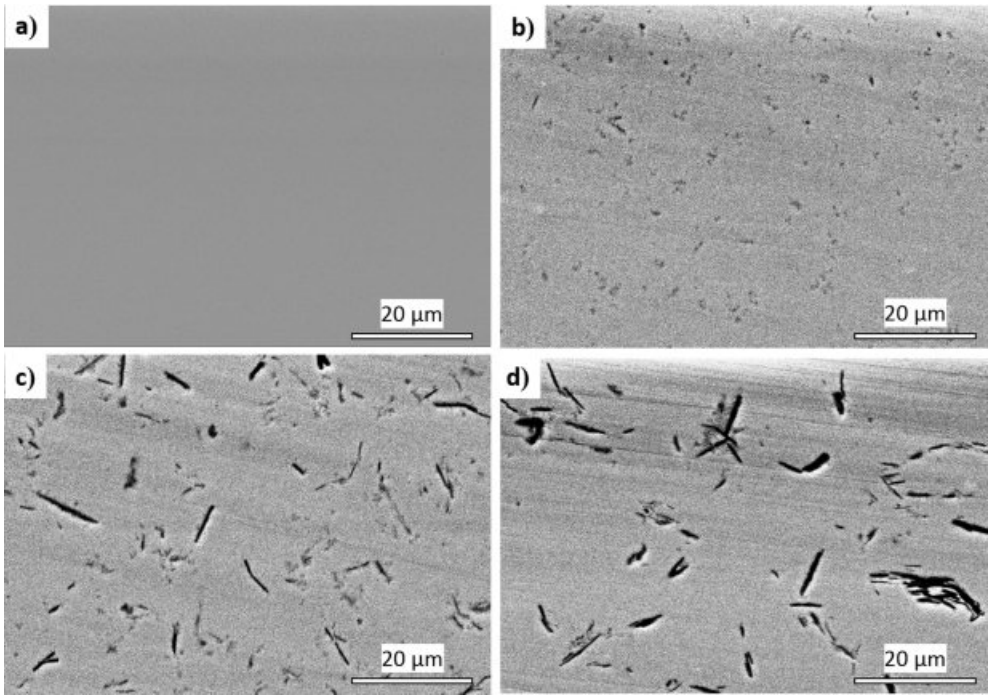

Fig. 3. SEM cross-sectional images of (a) pure Ni, (b) NiAl15BN5, (c) NiAl10BN10, and (d) NiAl5BN15 samples.

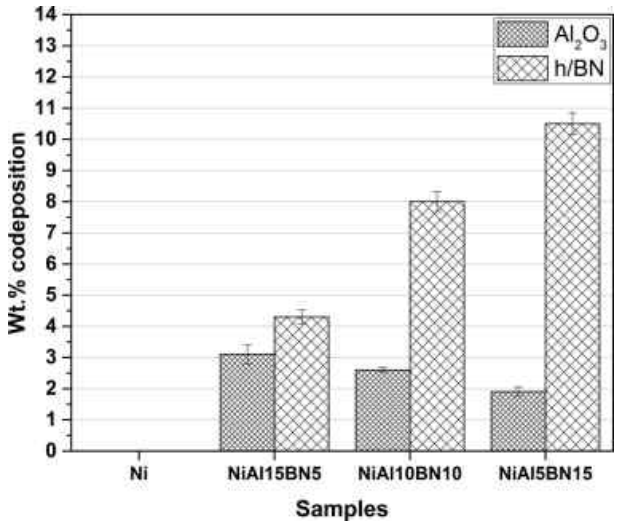

Fig. 4. Codeposition wt% of Al_2O_3 and h/BN into the coatings.

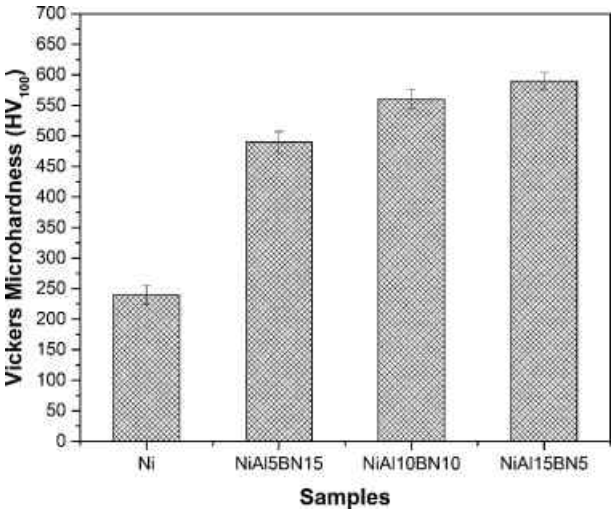

Fig. 5. Vickers microhardness of the samples.

of the coating was not significantly increased with increased content of h/BN. Unal et al. [20] have reported similar observations in their study on electrodeposited Ni-B/hBN composite coating where the microhardness values of Ni-B/hBN composite coatings were higher than pure Ni coatings, but lower than Ni-B alloy coatings. Hence, the study shows that the codeposition of Al_2O_3 is primarily responsible for the enhancement of the microhardness of the coating. The outcome is also supported by the cross-sectional view of the coatings, where an increase in h/BN content promoted the agglomerated clusters of h/BN nanosheets (Fig. 3(d)). In addition, as compared to Al_2O_3 nanoparticles, h/BN nanosheet has higher surface aspect ratio and further clustering of these nanosheets deteriorates the load bearing capacity.

Tribological properties

Tribological properties of Ni and Ni-Al_2O_3-h/BN composite coatings were evaluated by performing reciprocal dry sliding wear and coefficient of friction (COF) tests under fixed and variable loads.

Effect of Al_2O_3 and h/BN on friction and wear behaviors of the coatings

Variations of the coefficient of friction of Ni and Ni-

Al_2O_3-h/BN composite coatings under fixed 5 N load are shown in Fig. 6. Initially, the coefficient of friction started with higher values in all samples and then decreased gradually until sliding for 1 min. After a min of sliding time, the COF again increased slightly and maintained more or less constant values throughout the sliding time. The higher values of the coefficient of friction at initial sliding might be due to the surface asperity in contact between sliding ball and the flat specimen. As soon as the contact surfaces have worn out to fit the surface irregularities, the COF maintained the steady state value. Among the samples, Ni coating has shown the higher values of the COF, followed by NiAl15BN5 sample. As the content of h/BN is increased in the composite coatings, the average values of the COF decreased gradually. However, there is only a slight difference in the average values of the coefficient of friction in between NiAl10BN10 and NiAl5BN15 samples, although the content of h/BN is higher in the NiAl5BN15 sample. As seen from the SEM cross-sectional images in Fig. 3, NiAl10BN10 sample possessed well distribution of both Al_2O_3 nanoparticles and h/BN nanosheets, whereas, NiAl5BN15 sample possessed some agglomerated bundles of h/BN nanosheets. The uneven distribution of h/BN with agglomeration might be the possible reason for this significance. Uniform distribution of reinforced particles plays a crucial role in decreasing coefficient of friction. The h/BN has been well known for the solid lubricant material. Due to its layered sheet structure, the friction force is reduced upon sliding over it. Therefore, 2D materials such as h/BN, MoS_2, RGOs, WS_2, etc. have been studied for manufacturing solid-lubricating composites materials [19, 23, 24].

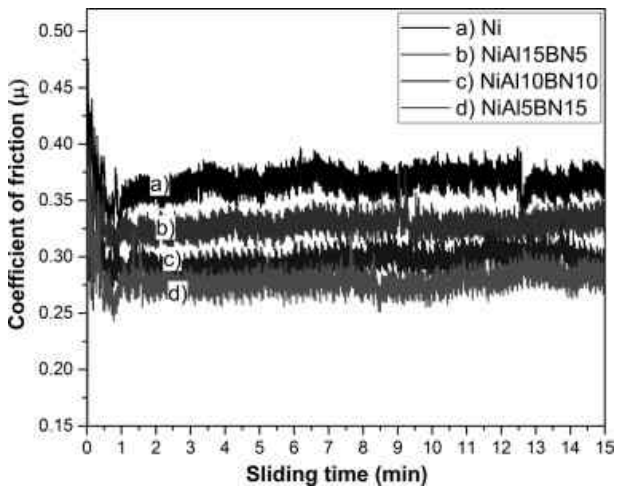

Fig. 6. Variation of the coefficient of frictions of different samples under 5 N applied load.

To investigate the worn out surface of the samples after the wear test, SEM observation was performed. Fig. 7(a-d) show the full scale worn out surfaces after wear test while their corresponding higher magnification images are shown in Fig. 7(e-h). As seen from the track width, the least width (~380 μm) of the wear track was found in NiAl15BN5 sample, where the content of Al_2O_3 is higher as compared to other samples. On the other hand, the highest width of the wear track (~560 μm) was measured in NiAl5BN15 sample. Ni coating shows a semicircular depth profile of the wear track, unlike Ni-Al_2O_3-h/BN composite coatings. The smaller width of the NiAl15BN5 coating might be ascribed to the higher hardness of the coating due to the dispersion hardening effect of the Al_2O_3 nanoparticles [18]. However, in h/BN rich samples, NiAl10BN10 and NiAl5BN15, the hardness values were not significantly increased. As a result, the width of the wear tracks is relatively larger. Fig. 7(e-h) demonstrate that all the samples possess abrasive nature of wear revealed by delamination and plow out of materials. As the ZrO_2 counter ball is significantly harder than the mating substrate, a transferred film from ZrO_2 ball to the substrate was not observed.

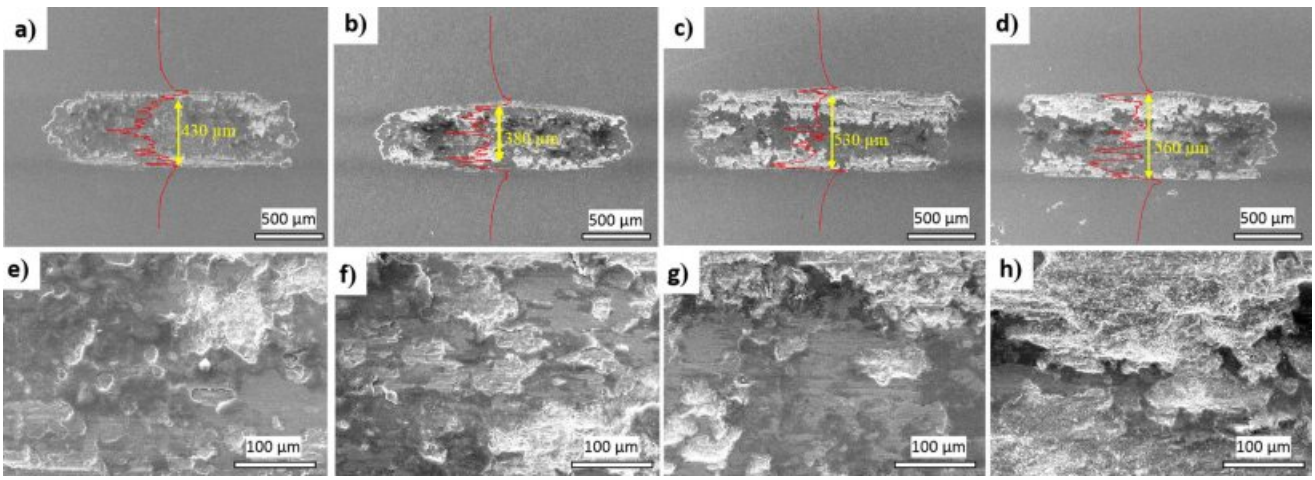

Fig. 7. SEM images of the worn surfaces after the wear test of the samples.

Effect of applied load on COF of the coating

To study the effect of applied load on COF, NiAl10BN10 was taken as a reference sample and carried out the tribology test under 3 N, 5 N, 7.5 N and 10 N normal loads. Fig. 8 shows the variation of coefficient friction with respect to different applied loads. A slight variation in coefficient of friction was observed under different loads. Higher values of the average COF was observed at 3 N load. Whereas, the lowest COF was measured at 5 N load. In addition to the presence of h/BN solid lubricant, the formation of an oxidative film and third body lubricity due to smashed wear debris at 5 N load might have played a vital role in decreasing the coefficient of friction. Beyond 5 N normal load, the COF increased slightly. Increase in normal load might have increased the abrasion rate. Furthermore, roughening of the substrate and possibly the formation of larger wear debris resulted the increased friction force. As a result, a higher coefficient of friction was observed at elevated normal loads. Hence, the optimum normal load was found to be 5 N based on the lowest coefficient of friction. Similarly, SEM images of the worn surfaces after the tribology test under different normal loads and their corresponding EDS spectra are shown in Fig. 9. A magnified view of the wear tracks (Fig. 9(e-h)) revealed that at 3 N and 5 N loads, similar nature of the abrasive wear was observed. It is interesting to note that although the similar nature of worn surfaces was observed at 3 N and 5 N loads, a low volume fraction of the plow out of materials were observed at 5 N normal load. The outcome is also supported by the lower coefficient of friction at this normal load. However, at higher loads (7.5 N and 10 N), larger flakes of the worn out debris were produced. Some micro-cracks were also observed within the wear tracks at higher loads. The EDS spectra (Fig. 9(i-l)) show a gradual increase in Zr and O contents in the wear debris at higher loads. Increased oxygen content might also be a consequence of the produced oxidative film in addition to the oxygen from the transferred ZrO_2 film.

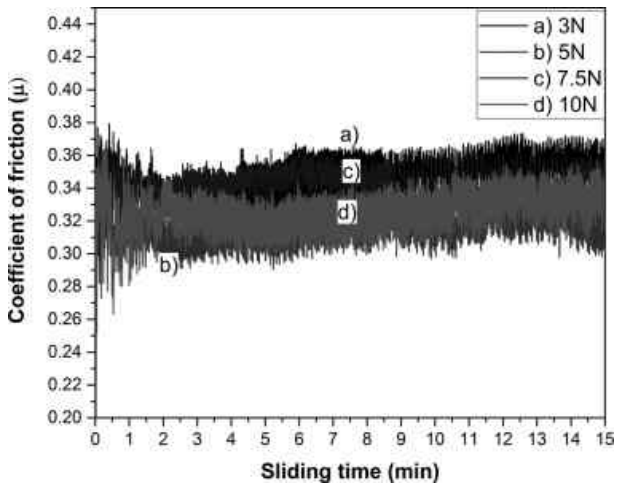

Fig. 8. Variation of the coefficient of friction under different applied loads in NiAl10BN10 sample.

Conclusion

Ni-Al_2O_3-h/BN composite coatings were successfully prepared by composite electrodeposition technique.

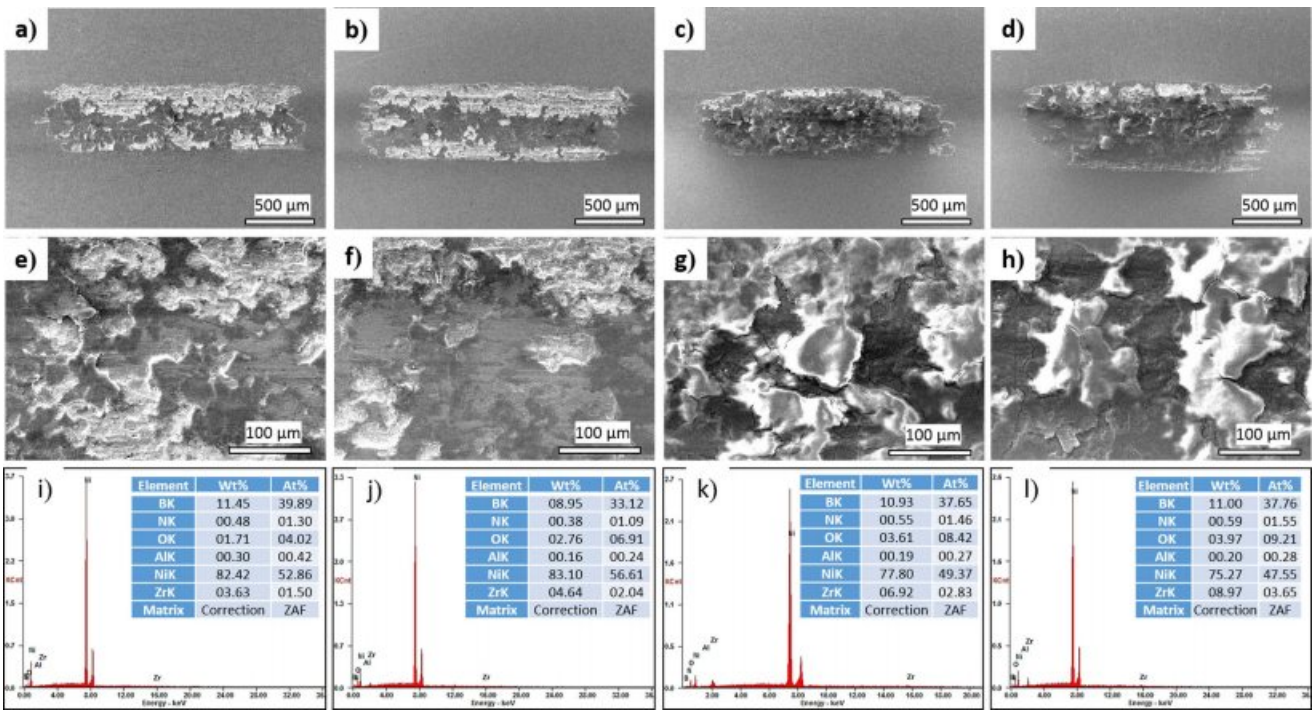

Fig. 9. SEM images and EDS spectra of the worn surfaces of NiAl10BN10 sample after wear test under different applied loads.

XRD analysis revealed the attenuation of (200) main reflection peak, indicating a less preferred orientation of the nickel crystallites in the composite coating. Vickers microhardness values of the composite coatings increased as compared to the pure nickel coating. The effect was more pronounced with codeposited Al_2O_3 than the h/BN. On the other hand, the coefficient of friction was decreased by increasing the content of h/BN in the deposit. In the Ni-Al_2O_3-h/BN composite coating, a combination of Al_2O_3 nanoparticles and h/BN nanosheets (10 g/L each) revealed the best performance to improving microhardness and the coefficient of friction. Furthermore, a tribology test under different normal loads exhibited the lowest values of the coefficient of friction at 5 N normal load.

Acknowledgement

This research was supported by the "International standardization of nickel-phosphorous ceramics electroless composite plating for industrial use" program through the "Korea Evaluation Institute of Industrial technology" of Korea funded by the Ministry of Science, ICT and Future planning (Grant number: 10080067).

References

1. G. Gyawali, R. Adhikari, H.S. Kim, H.-B. Cho, and S.W. Lee, ECS Electrochem. Lett. 2 (2012) C7-C10.
2. Nickel Plating Handbook, Nickel Institute Brussels, Belgium, 2014.
3. R. Casati and M. Vedani, Metals (Basel). 4 (2014) 65-83.
4. D. MIRACLE, Compos. Sci. Technol. 65 (2005) 2526-2540.
5. Z. Mahidashti, M. Aliofkhazraei, and N. Lotfi, Trans. Indian Inst. Met. 71 (2018) 257-295.
6. G. Gyawali, H.-S. Kim, K. Tripathi, T.-H. Kim, and S.W. Lee, J. Mater. Sci. Technol. 30 (2014) 796-802.
7. M. Srivastava, V.K. William Grips, and K.S. Rajam, Mater. Lett. 62 (2008) 3487-3489.
8. L. Benea, J. Appl. Electrochem. 39 (2009) 1671-1681.
9. F. Xia, H. Xu, C. Liu, J. Wang, J. Ding, and C. Ma, Appl. Surf. Sci. 271 (2013) 7-11.
10. V. Medelien, Surf. Coat. Technol. 154 (2002) 104-111.
11. J. Jiang, H. Chen, L. Zhu, W. Qian, S. Han, H. Lin, and H. Wu, RSC Adv. 6 (2016) 109001-109008.
12. H. Zhao, L. Liu, W. Hu, and B. Shen, Mater. Des. 28 (2007) 1374-1378.
13. G. Gyawali and S.W. Lee, J. Ceram. Process. Res. 16 (2015) 213-217.
14. L. Shi, C. Sun, and W. Liu, Appl. Surf. Sci. 254 (2008) 6880-6885.
15. I. Tudela, A.J. Cobley, and Y. Zhang, Friction 7, (2019) 169-180.
16. L. Chen, L. Wang, Z. Zeng, and J. Zhang, Mater. Sci. Eng. A 434 (2006) 319-325.
17. J.N. Balaraju, Kalavati, and K.S. Rajam, Surf. Coat. Technol. 200 (2006) 3933-3941.
18. H. Gül, F. Kiliç, S. Aslan, A. Alp, and H. Akbulut, Wear 267 (2009) 976-990.
19. Z. Shahri, S.R. Allahkaram, and A. Zarebidaki, Appl. Surf. Sci. 276 (2013) 174-181.
20. E. Ünal and H. Karahan, Surf. Coat. Technol. 333 (2018) 125-137.
21. Q. Feng, T. Li, H. Yue, K. Qi, F. Bai, and J. Jin, Appl. Surf. Sci. 254 (2008) 2262-2268.
22. T. Lampke, B. Wielage, D. Dietrich, and A. Leopold, Appl. Surf. Sci. 253 (2006) 2399-2408.
23. I. Sivandipoor and F. Ashrafizadeh, Appl. Surf. Sci. 263 (2012) 314-319.
24. M.F. Cardinal, P.A. Castro, J. Baxi, H. Liang, and F.J. Williams, Surf. Coat.Technol. 204 (2009) 85-90.